MAGNETIC RESONANCE

Hyperfine interaction of individual atoms on a surface

Philip Willke[1,2,3], Yujeong Bae[1,2,3], Kai Yang[1], Jose L. Lado[4,5], Alejandro Ferrón[6], Taeyoung Choi[2,3], Arzhang Ardavan[7], Joaquín Fernández-Rossier[4*], Andreas J. Heinrich[2,3]†, Christopher P. Lutz[1]†

Taking advantage of nuclear spins for electronic structure analysis, magnetic resonance imaging, and quantum devices hinges on knowledge and control of the surrounding atomic-scale environment. We measured and manipulated the hyperfine interaction of individual iron and titanium atoms placed on a magnesium oxide surface by using spin-polarized scanning tunneling microscopy in combination with single-atom electron spin resonance. Using atom manipulation to move single atoms, we found that the hyperfine interaction strongly depended on the binding configuration of the atom. We could extract atom- and position-dependent information about the electronic ground state, the state mixing with neighboring atoms, and properties of the nuclear spin. Thus, the hyperfine spectrum becomes a powerful probe of the chemical environment of individual atoms and nanostructures.

The hyperfine interaction between an electron and a nuclear spin provides insight into the electronic structure and chemical bonding of atoms, molecules, and solids. It is also key to realizing quantum operations of the nuclear spin (*1*–*3*). Although most experiments rely on ensemble measurement, detection and control of single nuclear spins is possible for diluted molecules in crystals (*4*), molecules in break junctions (*3*, *5*), ion traps (*2*), and defects in solids (*6*, *7*). Nevertheless, until now, no experimental tool allowed for imaging of the atomic-scale environment of the nucleus and simultaneous resolution of the hyperfine spectrum, which crucially depends on the local electronic structure.

Atomic resolution, along with atom manipulation, has been achieved by scanning probe methods, and they have been used to study the local electronic structure of atoms and molecules. Scanning probes allow chemical identification (*8*) and imaging of chemical bonds (*9*), and they provide access to the structure (*10*) and dynamics (*11*, *12*) of electron spins. The nuclear properties detected in scanning tunneling microscopy (STM) include changes in vibrational (*13*) and rotational (*14*) motion, but the hyperfine interaction has not previously been resolved owing to a limited resolution in energy (*15*, *16*).

Combining STM with electron spin resonance (ESR), as demonstrated for individual iron (Fe) (*17*, *18*) and titanium (Ti) atoms (*19*, *20*), potentially provides the required energy resolution. However, no hyperfine splitting was reported so far. For atoms that have low natural abundances of magnetic nuclei (such as Fe) or multiple magnetic isotopes (such as Ti), it is necessary to study a large number of individual atoms to establish the hyperfine physics. Here we present such a study, aided by a new understanding of the tunneling parameters (*21*) that improve the signal-to-noise ratio compared to previous ESR-STM experiments (*17*, *18*).

Individual Fe and Ti atoms from sources that have natural isotopic abundance were deposited on two atomic layers of MgO grown on silver (*22*). First, we examined Fe atoms adsorbed onto an oxygen binding site of the MgO (*23*) (Fig. 1A). We resonantly excited transitions between the electronic ground state (spin-up) and the first excited state (spin-down) of the Fe atom by using ESR. We used a magnetic field B = 0.9 T and a temperature T = 1.2 K, unless stated otherwise. This excitation led to a change in tunnel current ΔI when driven at the resonance frequency (*17*) (Fig. 1B). A magnetic tip was used for magnetoresistive readout, leading to different conductance for the two electronic states.

For 3.4% of Fe atoms (5 out of 147, see inset in Fig. 1B) investigated, the ESR peak was split by Δf = 231 ± 5 MHz, where f is the frequency of the applied radio frequency voltage. We attributed this splitting to the presence of a nuclear moment $I = {}^1/_2$ for ^{57}Fe (2.1% natural abundance). By contrast, the I = 0 isotopes, predominantly ^{56}Fe, showed no splitting. We could not distinguish different I = 0 isotopes and thus label them ^{56}Fe for simplicity. Because the hyperfine splitting Δf is much smaller than the thermal energy $k_BT/h \approx 25$ GHz, where k_B is the Boltzmann constant and h is the Planck constant, the two nuclear states $m_I = \pm{}^1/_2$ are occupied with equal probability. Thus, the ^{57}Fe peaks each had half the ESR peak height of the single peak observed for ^{56}Fe. Moreover, the simultaneous presence of two peaks indicates that the nuclear spin relaxation time was here much shorter than the time scale of the measurement (~1 ms) (*22*).

For the magnetic field used here, the electronic Zeeman energy is large compared to the hyperfine interaction. Because the Fe atom on MgO shows a large out-of-plane magnetic anisotropy, the electron spin is quantized along the out-of-plane direction z (*23*). Thus, the nuclear spin was quantized along z as well, leading to the spin Hamiltonian (*24*)

$$H = g_z\mu_B B_z S_z + A_z I_z S_z \quad (1)$$

where μ_B is the Bohr magneton and S_z and I_z are the z-axis spin operators for the electron and nuclear spin, respectively. Parameters g_z and A_z are the z components of the electron g-factor and the hyperfine coupling constant, respectively. B_z is the z component of the magnetic field. The very small nuclear Zeeman energy is neglected here.

When determining the eigenstates of Eq. 1, the spins can either be aligned or anti-aligned with the magnetic field to give product states $|m_S, m_I\rangle$, where m_S and m_I are the electron and nuclear quantum numbers (Fig. 1C). Transitions occurred between the m_S = ±2 electronic states (Δm_S = 4) (*17*) and left the nuclear spin state unchanged (Δm_I = 0), leading to one resonance peak for ^{56}Fe. The spectra were centered at frequency f_0 given by the Zeeman energy $hf_0 = g_z\mu_B B_z \Delta m_S$. The two frequencies observed for ^{57}Fe in Fig. 1B differed because of the relative alignment of the electron and nuclear spin, to give a peak splitting $\Delta f = \Delta m_S \Delta m_I A_z = 4A_z$, where $\Delta m_I = 1$ (*24*).

In contrast to that of Fe, the hyperfine interaction of Ti atoms was more complex and reflected changes in the local electronic environment (*24*). The Ti atoms studied here were hydrogenated (*19*), resulting in an electronic spin of ${}^1/_2$ that lacked magnetic anisotropy. Thus, to good approximation, the electron spin followed the magnetic-field direction (*19*, *20*). The hyperfine spectra for Ti located on a bridge binding site (Ti_B) of MgO (*20*) (Fig. 2) showed $2I + 1$ peaks, one for each nuclear spin state, resulting in six peaks for ^{47}Ti ($I = {}^5/_2$, 7.4% natural abundance), eight peaks for ^{49}Ti ($I = {}^7/_2$, 5.4%), and a single peak for the nuclear spin–free isotopes, predominantly ^{48}Ti (I = 0, 73.7%). We found a splitting Δf between adjacent peaks of ~47 MHz for both ^{47}Ti and ^{49}Ti, implying that their nuclear gyromagnetic ratios were equal [see section 2 in (*22*)]. For all investigated atoms, we found no appreciable dependence of the hyperfine splitting on the magnetic field caused by the proximity of

[1]IBM Almaden Research Center, San Jose, CA 95120, USA. [2]Center for Quantum Nanoscience, Institute for Basic Science (IBS), Seoul 03760, Republic of Korea. [3]Department of Physics, Ewha Womans University, Seoul 03760, Republic of Korea. [4]QuantaLab, International Iberian Nanotechnology Laboratory (INL), 4715-310 Braga, Portugal. [5]Institute for Theoretical Physics, ETH Zurich, 8093 Zurich, Switzerland. [6]Instituto de Modelado e Innovación Tecnológica (CONICET-UNNE), Facultad de Ciencias Exactas, Naturales y Agrimensura, Universidad Nacional del Nordeste, W3404AAS Corrientes, Argentina. [7]Centre for Advanced Electron Spin Resonance, Clarendon Laboratory, Department of Physics, University of Oxford, Oxford OX1 3PU, UK.
*On leave from Departamento de Física Aplicada, Universidad de Alicante, San Vicente del Raspeig 03690, Spain.
†Corresponding author. Email: cplutz@us.ibm.com (C.P.L.); heinrich.andreas@qns.science (A.J.H.)

the tip (*19*) nor on the local electric field induced by the dc bias voltage.

In contrast to ensemble measurements, the binding site of individual atoms could be determined from STM images, and the atom could be moved among binding sites by using atom manipulation. We moved a ^{47}Ti atom to different binding sites (Fig. 3A). We observed a pronounced reduction of the splitting Δf to ~10 MHz (Fig. 3B) when the Ti atom was moved from a bridge to an oxygen site (Ti_O). The larger splitting was restored by moving the same atom back to a bridge binding site. In Fig. 3C, we show the exact position of the atoms obtained from Fig. 3A and show density functional theory (DFT) calculations (*22*) of the respective electronic ground state. The statistics for different atoms on the same type of binding site (Fig. 3D) revealed a small, but reproducible, difference in Δf for the two inequivalent bridge binding sites. This difference was caused by different values of $g_x \neq g_y$ and $A_x \neq A_y$ (resulting from the low symmetry of the bridge binding site) along with a magnetic field direction $B_x \neq B_y$ [Fig. 3C and section 1 in (*22*)].

Hyperfine spectra for both isotopes of Ti_O are shown in high resolution in Fig. 3E. In addition to the strong decrease in Δf compared with that for Ti_B, the interval between peaks as well as their amplitudes were nonuniform. To describe the spectra, we generalize the hyperfine Hamiltonian in Eq. 1 to

$$H = H_{EZ} + H_{HF} + H_{NQ} \quad (2)$$

Here, the electron Zeeman term $H_{EZ} = \mu_B \sum_{i=x,y,z} g_i B_i S_i$ and the hyperfine term $H_{HF} = \sum_{i=x,y,z} A_i I_i S_i$ were generalized to include the x and y spin components, needed for electronic spins lacking strong anisotropy (*19*), and the hyperfine interaction was allowed to have anisotropy. Moreover, $H_{NQ} = \sum_{i=x,y,z} P_i I_i^2$ is the nuclear electric quadrupole interaction, caused by the electric field gradient at the position of the nucleus (*24*), where P_i are the components of the nuclear electric quadrupole tensor (*22*). This quadrupole term is irrelevant for $I = 1/2$ systems, as in the case of Fe (*24*). Using the known symmetry of the system, only three fit parameters, A_z, $A_x = A_y$, and P_z were required to give good fits to the complex hyperfine spectrum of Ti_O (*22*).

Simulated ESR spectra of the experimental data obtained by using EasySpin (*25*) are superimposed on the data in Fig. 3E. The fits reflect that the hyperfine and the nuclear quadrupole interaction have comparable energies for Ti_O, resulting in peaks that are irregularly spaced because they are not well approximated by eigenstates of either operator alone. Furthermore, these measurements allowed us to determine the ratio of the nuclear quadrupole moments of $^{49}Q/^{47}Q \approx 0.79$. The excellent agreement with ensemble measurements [$^{49}Q/^{47}Q = 0.82$ (*26*)] shows the fidelity of the model and that good accuracy was obtained with this limited number of fit parameters.

Although the electric quadrupole interaction changed the peak intensities and spacings for Ti_O, the overall reduction in Δf compared to that for Ti_B was caused by the reduction in the hyperfine coupling constant $\boldsymbol{A}$. We consider here two contributions (*24*). The first is the isotropic Fermi contact term originating from a finite spin density of unpaired s electrons at the nucleus induced by interaction with the d electrons. The second is the anisotropic magnetic dipolar interaction of the nuclear spin with the surrounding d electrons, which depends on the orbital symmetry (*27*). The observed changes in Δf for the different binding sites of Ti were caused by the occupation of different orbitals in the magnetic ground state of the atom (Fig. 3C). We found a larger Fermi contact contribution for Ti_B (+50 MHz) compared with that for Ti_O (+19 MHz), presumably caused by a difference in covalency (*24*) [section 2 in (*22*)].

More importantly, the three spatial components of the dipolar contribution changed in magnitude and sign for the different binding sites. Because the magnetic field was applied

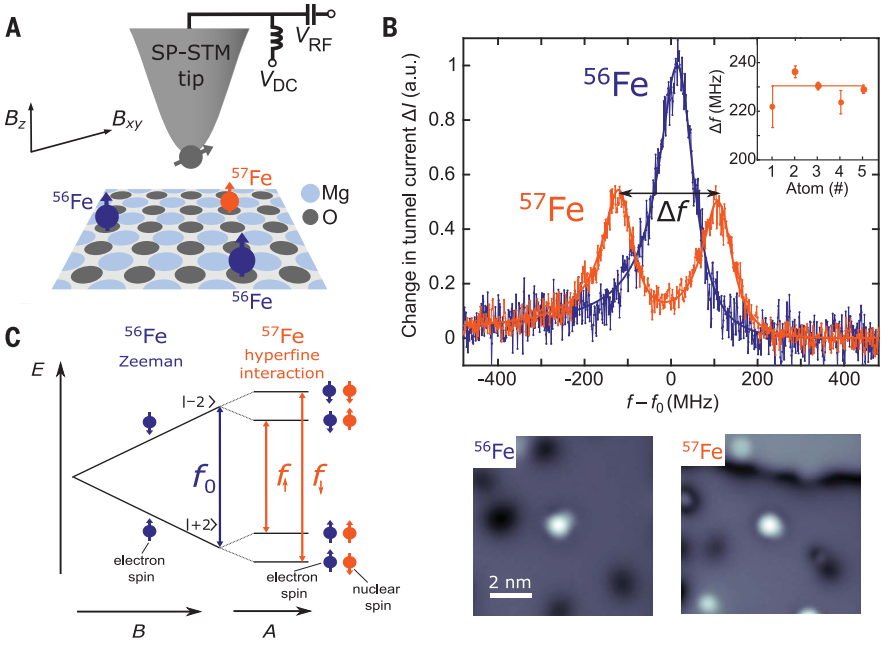

Fig. 1. Hyperfine interaction studied by ESR in a scanning tunneling microscope. (**A**) Experimental setup showing different isotopes of single Fe atoms on a bilayer MgO film on Ag(001) in an STM (B = 0.9 T, B_z = 0.1 T, and T = 1.2 K). ESR was performed by applying a radio frequency voltage (V_{RF}) to the tunneling junction (*17*, *18*). SP, spin-polarized; V_{DC}, direct current voltage. (**B**) ESR spectra of the change in tunnel current for different Fe isotopes (top). The blue line shows Fe that has zero nuclear spin (likely ^{56}Fe; see main text). The orange line shows ^{57}Fe with nuclear spin $I = 1/2$. Spectra were normalized to unity for ^{56}Fe and given in arbitrary units (a.u.). Electron Zeeman energy gives the center frequency f_0, here 19.89 GHz for ^{56}Fe and 19.87 GHz for ^{57}Fe (tunnel conditions: I_{set} = 12 pA, V_{DC} = 60 mV, and V_{RF} = 60 mV). The inset shows the peak splitting Δf for five different ^{57}Fe atoms. The solid line indicates the error-weighted mean. Shown at the bottom are topographic images of both atoms. (**C**) Schematic of the energy levels E of the ^{56}Fe atom, compared to those of ^{57}Fe, including hyperfine interaction as a function of the external magnetic field B and the hyperfine constant A (the small nuclear Zeeman energy was neglected).

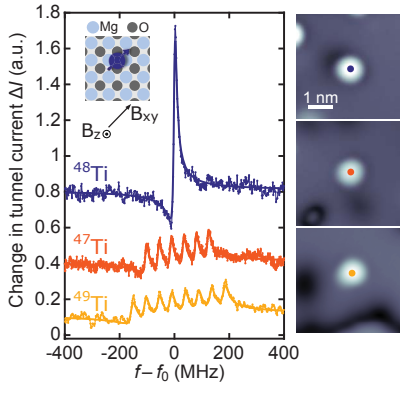

Fig. 2. Hyperfine interaction for titanium on a bridge binding site. On the left are ESR spectra for ^{48}Ti (blue, nuclear spin I = 0), ^{47}Ti (orange, $I = 5/2$) and ^{49}Ti (yellow, $I = 7/2$). The inset shows the bridge binding site. On the right are STM images for each atom. Experimental conditions for ^{48}Ti: f_0 = 23.03 GHz, I_{set} = 8 pA, V_{DC} = 40 mV, and V_{RF} = 30 mV; for ^{47}Ti: f_0 = 22.99 GHz, I_{set} = 8 pA, V_{DC} = 40 mV, and V_{RF} = 30 mV; and for ^{49}Ti: f_0 = 22.69 GHz, I_{set} = 20 pA, V_{DC} = 60 mV, and V_{RF} = 40 mV.

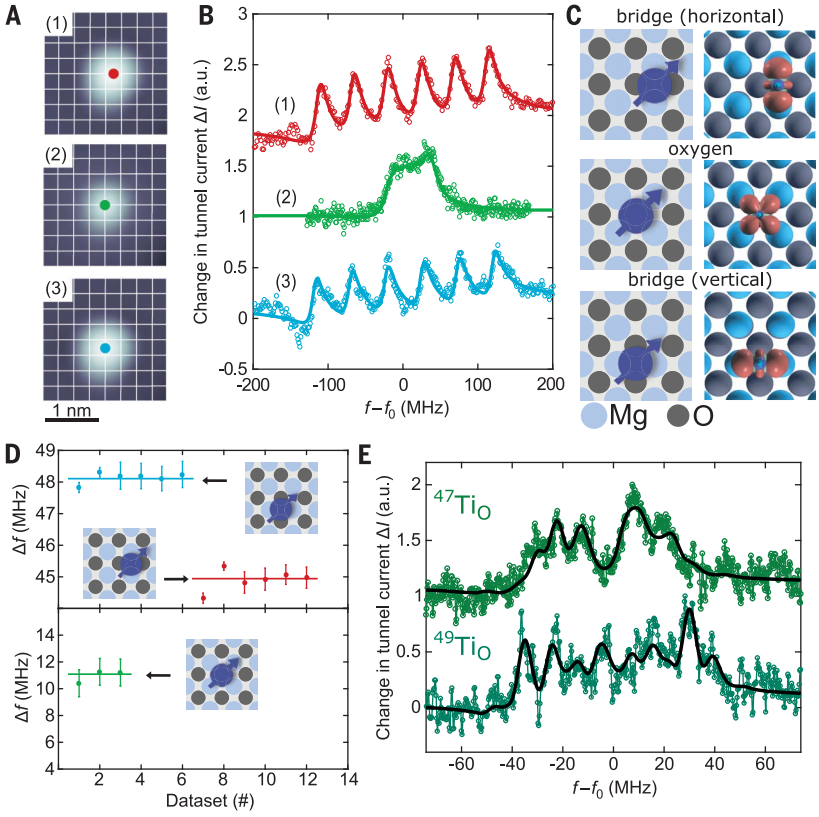

Fig. 3. Binding site dependence of the hyperfine spectrum of titanium. (**A**) By using atom manipulation, a ^{47}Ti atom on a bridge site (site 1, red, Ti_B) was moved to an oxygen binding site (site 2, green, Ti_O) and subsequently to a different bridge binding site (site 3, blue). White lines indicate the MgO lattice, with the intercepts corresponding to the positions of oxygen atoms. (**B**) ESR spectra for the binding sites in (A) (site 1: I_{set} = 10 pA, V_{DC} = 40 mV, V_{RF} = 40 mV, and f_0 = 22.89 GHz; site 2: I_{set} = 10 pA, V_{DC} = 60 mV, V_{RF} = 7 mV, and f_0 = 22.91 GHz; and site 3: I_{set} = 10 pA, V_{DC} = 40 mV, V_{RF} = 40 mV, and f_0 = 22.69 GHz). (**C**) Sketches (left) show the binding site. Calculated spin density (right) of the binding configurations obtained by DFT. (**D**) Statistics of the hyperfine splitting Δf for the different binding sites (horizontal bridge site in red, Δf = 44.9 ± 0.5 MHz; vertical bridge site in blue, Δf = 48.1 ± 0.3 MHz; and oxygen site in green, Δf = 10.8 ± 0.7 MHz. For the latter, Δf was obtained by neglecting electric quadrupole interaction which leads to unequal spacing of the peaks). (**E**) High-resolution ESR spectra for ^{47}Ti (top, I_{set} = 1.5 pA, V_{DC} = 60 mV, V_{RF} = 25 mV, T = 0.6 K, and f_0 = 22.49 GHz) and ^{49}Ti (bottom, I_{set} = 2.5 pA, V_{DC} = 60 mV, V_{RF} = 25 mV, T = 0.6 K, and f_0 = 22.49 GHz) on an oxygen binding site. Black lines are fits to the data, including the anisotropic hyperfine and nuclear electric quadrupole interaction (see main text).

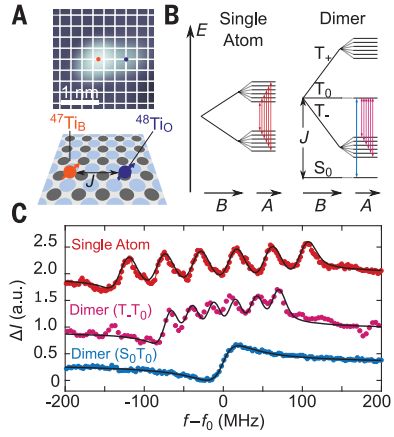

Fig. 4. Tuning the hyperfine splitting of a coupled two-atom nanostructure. (**A**) Topography of a dimer of Ti atoms created by atom manipulation (separation 7.2 Å). J denotes the exchange coupling strength between them. The bridge-site atom has a nuclear magnetic moment ($^{47}Ti_B$, $I = {}^5/_2$); the oxygen-site atom is nuclear spin–free ($^{48}Ti_O$, I = 0). (**B**) Energy levels of the single $^{47}Ti_B$ atom (left) and the dimer (right). For the dimer, the electronic spins form a singlet-triplet system because of exchange coupling (coupling strength J/h = 29.1 ± 0.2 GHz). (**C**) ESR spectrum of the transitions between T_0 and T_- taken on $^{47}Ti_B$ in the dimer reveals a decrease in hyperfine splitting Δf (middle, I_{set} = 10 pA, V_{DC} = 40 mV, V_{RF} = 20 mV, and f_0 = 22.89 GHz) compared with that of the isolated case (top, same data as in Fig. 2A). In the case of the singlet-triplet transition, S_0T_0, no hyperfine splitting was observed (bottom, I_{set} = 5 pA, V_{DC} = 40 mV, V_{RF} = 20 mV, and f_0 = 29.72 GHz).

nearly in-plane (Fig. 1A), the in-plane components A_x and A_y contributed the most to Δf. In the case of Ti_B, the dipolar contribution added to the Fermi contact part for one of the two components ($A_x \approx +61$ MHz; $A_y \approx +29$ MHz). By contrast, for Ti_O, both in-plane directions opposed the Fermi contact interaction, resulting in $A_x = A_y \approx +10$ MHz. As a result, Δf is smaller for Ti_O than for Ti_B. The strength of the hyperfine interaction and the importance of quadrupole interaction revealed the profound change in the chemical environment of the Ti atom upon moving it from a bridge site to an oxygen site: Modeling the hyperfine interaction and taking the DFT ground state into account, we find that the bonding with oxygen reduces the electron spin density at the Ti nucleus for Ti_O [~−1 instead of ~−2.8 atomic units for Ti_B (*22*)]. Moreover, the radial spread of the spin-polarized orbital $\langle r^{-3} \rangle$ can be deduced from the hyperfine splitting and the electric quadrupole contribution, which lies at ~(0.5 Å)$^{-3}$ for both binding sites (*22*).

Hyperfine spectra can also reveal changes in the magnetic environment, as we demonstrate here using assembled structures of Ti atoms. Figure 4A shows a $^{47}Ti_B$ atom with a nuclear spin $I = {}^5/_2$ that was moved to a position ~7 Å from a $^{48}Ti_O$ atom (I = 0). Because of the exchange interaction between the electronic spins, an electronic singlet-triplet system was formed [right panel of Fig. 4B and section 3 in (*22*)] (*19*, *20*). The Zeeman term split the triplet states (T_-, T_0, and T_+), whereas the energies of both the singlet S_0 and the triplet state T_0 remained independent of magnetic field.

Analogously, the hyperfine interaction did not split either S_0 or T_0, and for the T_+ and T_- states, the splitting remained the same as for the single atom (Fig. 4B). Thus, the hyperfine splitting for the T_-T_0 transition, which involved one of the magnetic field–independent states (T_0), decreased to only 27.2 ± 0.4 MHz, roughly half the value of the isolated Ti case (Fig. 4C). Accordingly, the hyperfine splitting of the singlet-triplet transition (S_0T_0) in Fig. 4C was essentially zero (less than our ~10 MHz linewidth). These transitions allowed us to probe the polarization of the coupled-atom states and to quantify the degree of state mixing to 87% in the singlet state [section 3 in (*22*)]. Here $\boldsymbol{A}$ remained constant, and instead, the electronic spin magnetization was changed (*20*). This Ti dimer structure showed that the collective properties that emerged in a correlated multispin structure yielded characteristics sharply different than those of the constituents.

REFERENCES AND NOTES

1. B. E. Kane, *Nature* **393**, 133–137 (1998).
2. B. B. Blinov, D. Leibfried, C. Monroe, D. J. Wineland, *Quantum Inform. Process.* **3**, 45–59 (2004).

3. S. Thiele *et al*., *Science* **344**, 1135–1138 (2014).
4. J. Köhler, A. C. J. Brouwer, E. J. J. Groenen, J. Schmidt, *Science* **268**, 1457–1460 (1995).
5. R. Vincent, S. Klyatskaya, M. Ruben, W. Wernsdorfer, F. Balestro, *Nature* **488**, 357–360 (2012).
6. P. Neumann *et al*., *Science* **329**, 542–544 (2010).
7. J. J. Pla *et al*., *Nature* **496**, 334–338 (2013).
8. Y. Sugimoto *et al*., *Nature* **446**, 64–67 (2007).
9. L. Gross, F. Mohn, N. Moll, P. Liljeroth, G. Meyer, *Science* **325**, 1110–1114 (2009).
10. A. J. Heinrich, J. A. Gupta, C. P. Lutz, D. M. Eigler, *Science* **306**, 466–469 (2004).
11. S. Loth, M. Etzkorn, C. P. Lutz, D. M. Eigler, A. J. Heinrich, *Science* **329**, 1628–1630 (2010).
12. A. A. Khajetoorians *et al*., *Science* **339**, 55–59 (2013).
13. B. C. Stipe, M. A. Rezaei, W. Ho, *Science* **280**, 1732–1735 (1998).
14. F. D. Natterer, F. Patthey, H. Brune, *Phys. Rev. Lett.* **111**, 175303 (2013).
15. F. Delgado, J. Fernández-Rossier, *Phys. Rev. Lett.* **107**, 076804 (2011).
16. C. R. Ast *et al*., *Nat. Commun.* **7**, 13009 (2016).
17. S. Baumann *et al*., *Science* **350**, 417–420 (2015).
18. W. Paul, S. Baumann, C. P. Lutz, A. J. Heinrich, *Rev. Sci. Instrum.* **87**, 074703 (2016).
19. K. Yang *et al*., *Phys. Rev. Lett.* **119**, 227206 (2017).
20. Y. Bae *et al*., arXiv:1807.04322 [cond-mat.mes-hall] (11 July 2018).
21. P. Willke *et al*., *Sci. Adv.* **4**, q1543 (2018).
22. Materials and methods are available as supplementary materials.
23. W. Paul *et al*., *Nat. Phys.* **13**, 403–407 (2017).
24. A. Abragam, B. Bleaney, *Electron Paramagnetic Resonance of Transition Ions* (Oxford Univ. Press, 2012).
25. S. Stoll, A. Schweiger, *J. Magn. Reson.* **178**, 42–55 (2006).
26. K. H. Channappa, J. M. Pendlebury, *Proc. Phys. Soc.* **86**, 1145–1146 (1965).
27. F. E. Mabbs, D. Collison, *Electron Paramagnetic Resonance of d Transition Metal Compounds* (Elsevier, 2013), vol. 16.

ACKNOWLEDGMENTS

We thank B. Melior for expert technical assistance and W. Paul, F. Natterer, and S. Fatayer for further discussions. **Funding:** We gratefully acknowledge financial support from the Office of Naval Research. P.W., Y.B., T.C., and A.J.H. acknowledge support from the Institute for Basic Science under grant IBS-R027-D1. A.F. acknowledges funding from CONICET (PIP11220150100327) and FONCyT (PICT-2012- 2866). J.L.L. is grateful for financial support from the ETH Fellowship program. J.F.-R. thanks the Fundação para a Ciência e a Tecnologia, under project no. PTDC/FIS-NAN/4662/2014 (016656). A.A. thanks the Engineering and Physical Sciences Research Council, under project no. EP/L011972/1. P.W. acknowledges support from the Alexander von Humboldt Foundation. **Author contributions:** A.J.H. and C.P.L. supervised the project. P.W., Y.B., K.Y., and T.C. carried out the STM measurements. P.W. performed the analysis and wrote the manuscript with help from all authors. A.F., J.L.L., and J.F.-R. performed the DFT calculations. All authors discussed the results and edited the manuscript. **Competing interests:** None declared. **Data and materials availability:** All data needed to evaluate the conclusions in the paper are present in the paper and/or the supplementary materials. Additional data related to this paper may be requested from the authors.

SUPPLEMENTARY MATERIALS

www.sciencemag.org/content/362/6412/336/suppl/DC1
Materials and Methods
Supplementary Text
Figs. S1 to S4
Table S1
References (*28*–*32*)

27 March 2018; accepted 15 August 2018
10.1126/science.aat7047

Hyperfine interaction of individual atoms on a surface

Philip Willke, Yujeong Bae, Kai Yang, Jose L. Lado, Alejandro Ferrón, Taeyoung Choi, Arzhang Ardavan, Joaquín Fernández-Rossier, Andreas J. Heinrich and Christopher P. Lutz

Science **362** (6412), 336-339.
DOI: 10.1126/science.aat7047

Hyperfine spectra of surface atoms

The interaction of nuclei with nonzero spin with electron spins creates small electronic energy. With a scanning tunneling microscope tip, Willke *et al.* measured these hyperfine interactions for iron and titanium atoms that were manipulated on a magnesium oxide surface. The tip was also used to measure electron paramagnetic resonance spectra. The hyperfine structure of single atoms was sensitive to the binding site of the atom as well as its position relative to other magnetic atoms.

Science, this issue p. 336